22 Diffusion and Conduction in Percolation Systems

Armin Bunde and Jan W. Kantelhardt

22.1 Introduction

Percolation is a standard model for disordered systems. Its applications range from transport in amorphous and porous media and composites to the properties of branched polymers, gels and complex ionic conductors. Because of universality the results do not depend on the specific model, and general scaling laws can be deduced. In this chapter we give a short introduction to percolation theory and describe one application to composites. We start with the structural properties of site percolation clusters and their substructures and report on other percolation systems after that. Then we turn to the dynamical properties of percolation clusters and discuss the way the laws of diffusion and conduction are modified on random fractal structures. Finally, we review a particular application of the percolation concept, transport in heterogeneous ionic conductors.

22.2 The (Site-)Percolation Model

Percolation represents the basic model for a structurally disordered system (for recent reviews see [1–3], for applications see [4, 5]). Let us consider a square lattice, where each site is occupied randomly with probability p or is empty with probability $1 - p$ (see Fig. 22.1). Occupied and empty sites may stand for very different physical properties. For illustration, let us assume that the occupied sites are electrical conductors, the empty sites represent insulators, and that electrical current can only flow between nearest-neighbour conductor sites.

At low concentration p, the conductor sites are either isolated or form small clusters of nearest-neighbour sites. Two conductor sites belong to the same cluster if they are connected by a path of nearest-neighbour conductor sites, and a current can flow between them. At low p values, the mixture is an insulator, since no conducting path connecting opposite edges of our lattice exists. At large p values, on the other hand, many conducting paths between opposite edges exist, where electrical current can flow, and the mixture is a conductor. At some concentration in between, therefore, a threshold concentration p_c must exist where for the first time electrical current can percolate

$p = 0.2$ $p = 0.59$ $p = 0.8$
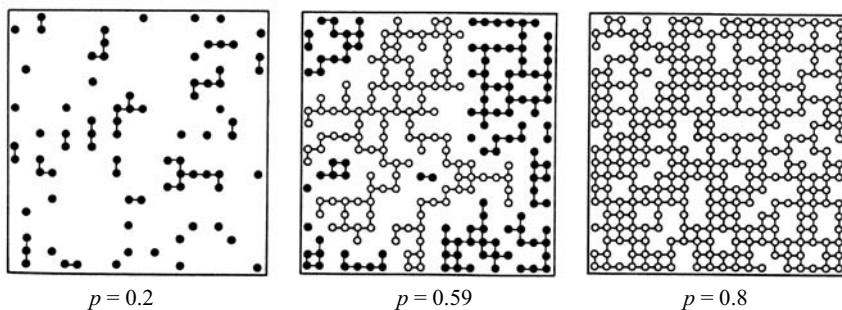
Fig. 22.1. Site percolation on the square lattice: The small circles represent the occupied sites for three different concentrations: $p = 0.2$, 0.59, and 0.80. Nearest-neighbour cluster sites are connected by lines representing the bonds. Filled circles are used for finite clusters, while open circles mark the large *infinite* cluster.

from one edge to the other. Below p_c we have an insulator, above p_c we have a conductor. The threshold concentration is called the percolation threshold, or, since it separates two different phases, the critical concentration.

If the occupied sites are superconductors and the empty sites are con-ductors, p_c separates a normal-conducting phase below p_c from a supercon-ducting phase above p_c. Another example is a mixture of ferromagnets and paramagnets, where the system changes at p_c from a paramagnet to a ferro-magnet.

In contrast to the more common thermal phase transitions, where the transition between two phases occurs at a critical temperature, the perco-lation transition described here is a geometrical phase transition, which is characterized by the geometric features of large clusters in the neighbour-hood of p_c. At low values of p only small clusters of occupied sites exist. When the concentration p is increased the average size of the clusters increases. At the critical concentration p_c a large cluster appears which connects opposite edges of the lattice. We call this cluster the *infinite* cluster, since its size diverges in the thermodynamic limit. When p is increased further the density of the infinite cluster increases, since more and more sites become part of the infinite cluster, and the average size of the *finite* clusters, which do not belong to the infinite cluster, decreases. At $p = 1$, trivially, all sites belong to the infinite cluster.

The critical concentration depends on the details of the lattice and in-creases, for fixed dimension d of the lattice, with decreasing coordination number z of the lattice: For the triangular lattice, $z = 6$ and $p_c = 1/2$, for the square lattice, $z = 4$ and $p_c \cong 0.592746$, and for the honeycomb lattice, $z = 3$ and $p_c \cong 0.6962$. For fixed z, p_c decreases if the dimension d is en-hanced. In both the triangular lattice and the simple cubic lattice we have $z = 6$, but p_c for the simple cubic lattice is considerably smaller, $p_c \cong 0.3116$.

Table 22.1. Critical exponents and fractal dimensions for percolation in two and three dimensions. The numerical values are taken from [1, 6, 7].

Quantity		Exp.	$d = 2$	$d = 3$
Order parameter	$P_\infty(p) \sim (p - p_c)^\beta$	β	$5/36$	0.417 ± 0.003
Correlation length	$\xi(p) \sim |p - p_c|^{-\nu}$	ν	$4/3$	0.875 ± 0.008
Cluster mass	$M(r) \sim r^{d_f}$	d_f	$91/48$	2.524 ± 0.008
Backbone mass	$M_B(r) \sim r^{d_B}$	d_B	1.6432 ± 0.0008	1.855 ± 0.015
Chemical Path	$\ell(r) \sim r^{d_{\min}}$	$d_{\min}$	1.1307 ± 0.0004	1.374 ± 0.004
Random Walk	$\langle r^2(t) \rangle \sim t^{2/d_w}$	d_w	2.871 ± 0.001	3.80 ± 0.02
Conductivity	$\sigma_{dc}(p) \sim (p_c - p)^\mu$	μ	1.310 ± 0.001	1.99 ± 0.01
Superconductivity	$\sigma_S(p) \sim (p - p_c)^{-s}$	s	1.310 ± 0.001	0.74 ± 0.03

The percolation transition is characterized by the geometrical properties of the clusters near p_c [1, 2]. The probability P_∞ that a site belongs to the infinite cluster is zero below p_c and increases above p_c as

$$P_\infty \sim (p - p_c)^\beta. \tag{22.1}$$

This behaviour is illustrated in Fig. 22.2. The linear size of the *finite* clusters, below and above p_c, is characterized by the correlation length ξ. The correlation length is defined as the mean distance between two sites on the same finite cluster and represents the characteristic length scale in percolation. When p approaches p_c, ξ increases as

$$\xi \sim |p - p_c|^{-\nu}, \tag{22.2}$$

with the same exponent ν below and above the threshold (see also Fig. 22.2). While p_c depends explicitly on the type of the lattice, the critical exponents β and ν are universal and depend only on the dimension d of the lattice, but not on the type of the lattice. The values of the critical exponents are given in Tab. 22.1 for two and three dimensions.

22.3 The Fractal Structure of Percolation Clusters near p_c

Near p_c on length scales smaller than ξ both the infinite cluster and the finite clusters are self-similar, i.e., if we cut a small part out of a large cluster, magnify it to the original cluster size and compare it with the original, we cannot tell the difference: Both look the same. This feature is illustrated in Fig. 22.3, where a large cluster at p_c is shown in four different magnifications.
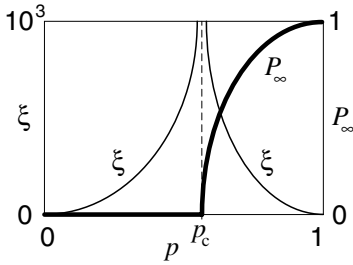
Fig. 22.2. Schematic diagram of the probability P_∞ (cf. (22.1), bold line) and the correlation length ξ (cf. (22.2), thin line) versus the concentration p of occupied sites.

We leave it to the reader to find out what is the original and what are the magnifications.

We have learnt in Chap. 19 that – as a consequence of the (non-trivial) self-similarity – the cluster is characterized by a "fractal" dimension, which is smaller than the dimension d of the embedding lattice. The mean mass of the cluster within a circle of radius r increases with r as

$$M(r) \sim r^{d_{\mathrm{f}}}, \quad r \ll \xi, \tag{22.3}$$

with the fractal dimension d_{f}. The numerical values of d_{f} can be found in Table 22.1. Above p_{c} on length scales *larger* than ξ the infinite cluster can be regarded as an homogeneous system which is composed of many cells of size ξ. Mathematically, this can be summarized as

$$M(r) \sim \begin{cases} r^{d_{\mathrm{f}}}, & \text{if } r \ll \xi, \\ r^{d}, & \text{if } r \gg \xi. \end{cases} \tag{22.4}$$

Fig. 22.4 shows a part of the infinite cluster above p_{c} ($p = 1.003\,p_{\mathrm{c}}$) on different length scales. At large length scales ($r \gg \xi$, upper left) the cluster appears homogeneous, while on lower length scales ($r \ll \xi$, lower pictures) the cluster is self-similar.

The fractal dimension d_{f} can be related to β and ν in the following way: Above p_{c}, the mass M_∞ of the infinite cluster in a large lattice of size L^d is proportional to $L^d P_\infty$. On the other hand, this mass is also proportional to the number of unit cells of size ξ, $(L/\xi)^d$, multiplied by the mass of each cell which is proportional to $\xi^{d_{\mathrm{f}}}$. This yields (with (22.1) and (22.2))

$$M_\infty \sim L^d P_\infty \sim L^d (p - p_{\mathrm{c}})^{\beta} \sim (L/\xi)^d \xi^{d_{\mathrm{f}}} \sim L^d (p - p_{\mathrm{c}})^{\nu d - \nu d_{\mathrm{f}}}, \tag{22.5}$$

and hence, comparing the exponents of $(p - p_{\mathrm{c}})$,

$$d_{\mathrm{f}} = d - \frac{\beta}{\nu}. \tag{22.6}$$

Since β and ν are universal exponents, d_{f} is also universal.

A fractal percolation cluster is composed of several fractal substructures, which are described by other exponents [1, 2]. Imagine applying a voltage
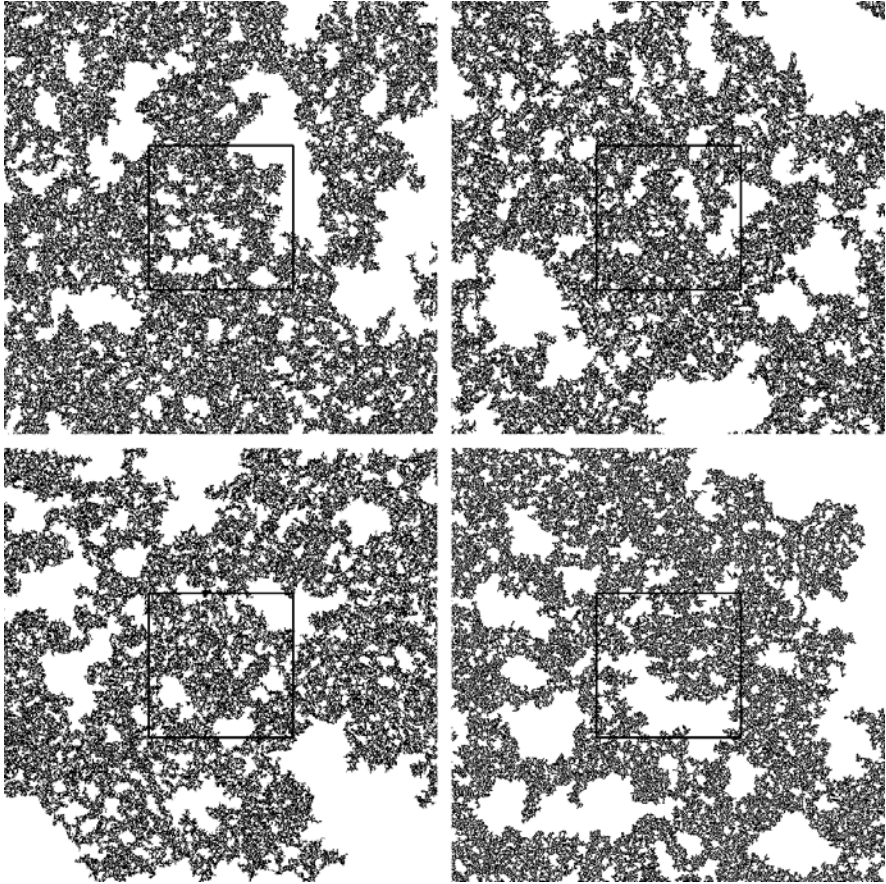
Fig. 22.3. Four successive magnifications of the incipient infinite cluster that forms at the percolation threshold on the square lattice. Three of the panels are magnifications of the center squares marked by black lines. In the figure that you see, however, the labels of the four panels have been removed and the panels have been scrambled. Attempt to put them back into sequence by eye – it is extremely difficult if the system is at the percolation threshold ($p = p_c$). An educational game is to time how long it takes each player to detect by eye which of the 24 possible orderings is the correct one that arranges the four panels in increasing order of magnification.
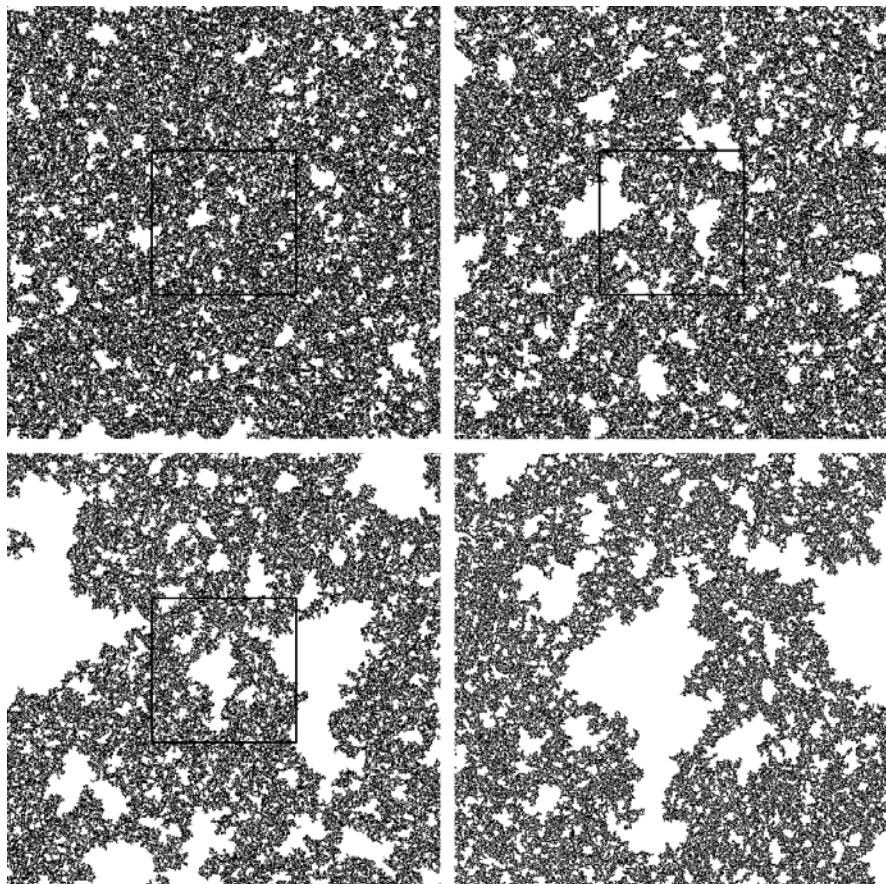
Fig. 22.4. The same as Fig. 22.3 except that now the system is slightly (0.3 %) above the percolation threshold and the panels are not scrambled. The upper left picture shows the original and the other pictures are magnifications of the center squares marked by black lines. The correlation length ξ is approximately equal to the linear size of the third (lower left) picture. When comparing the two lower pictures, the self-similarity at small length scales below ξ is easy to recognize.

between two sites at opposite edges of a metallic percolation cluster: The backbone of the cluster consists of those sites (or bonds) which carry the electric current. The topological distance between both points (also called chemical distance) is the length of the shortest path on the cluster connecting them. The dangling ends are those parts of the cluster which carry no current and are connected to the backbone by a single site only. The red bonds (or singly connected bonds), finally, are those bonds that carry the total current; when they are cut the current flow stops.
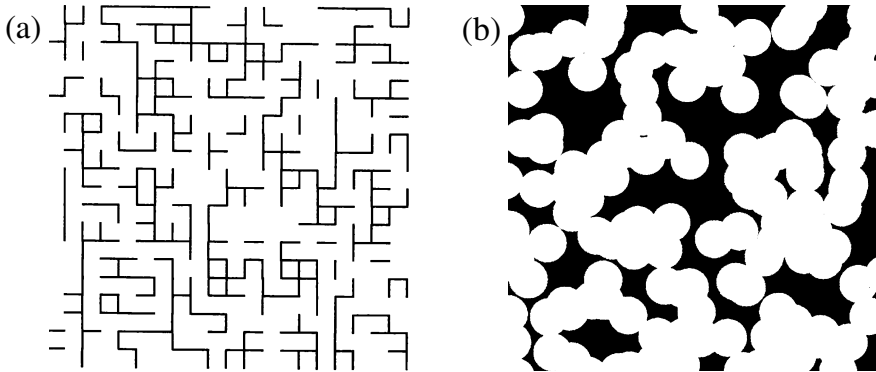
Fig. 22.5. Further percolation systems: (a) Bond percolation cluster on a square lattice and (b) continuum percolation of conductive material with circular holes of fixed radius at the percolation threshold.

The fractal dimension d_{B} of the backbone is smaller than the fractal dimension d_{f} of the cluster, reflecting the fact that most of the mass of the cluster is concentrated in the dangling ends. On the average, the topological length ℓ of the path between two points on the cluster increases with the Euclidean distance r between them as $\ell \sim r^{d_{\min}}$. The values of the fractal dimensions d_{B} and $d_{\min}$ are given in Table 22.1 for two and three dimensions. The fractal dimensions of the red bonds d_{red} are known from exact analytical arguments. The mean number of red bonds varies with p as $n_{\mathrm{red}} \sim (p - p_{\mathrm{c}})^{-1} \sim \xi^{1/\nu} \sim r^{1/\nu}$, and the fractal dimension of the red bonds is therefore $d_{\mathrm{red}} = 1/\nu$ [1].

A further important substructure of the cluster is the external perimeter (which is also called the hull). The hull consists of those sites of the cluster which are adjacent to empty sites and are connected with infinity via empty sites. It is an important model for random fractal interfaces. In two dimensions, the hull has the fractal dimension $d_{\mathrm{h}} = 7/4$, while its mass seems to be proportional to the mass of the cluster in $d = 3$, i.e. $d_{\mathrm{h}} = d_{\mathrm{f}}$. In contrast to the hull, the total perimeter also includes the holes in the cluster.

22.4 Further Percolation Systems

So far we have considered site percolation, where the sites of a lattice have been occupied randomly. When the sites are all occupied, but the bonds between the sites are randomly occupied with probability q, we speak of bond percolation (see Fig. 22.5 (a)). Two occupied bonds belong to the same cluster if they are connected by a path of occupied bonds, and the critical concentration q_{c} of bonds ($q_{\mathrm{c}} = 1/2$ in the square lattice and $q_{\mathrm{c}} \simeq 0.2488$ in

the simple cubic lattice) separates a phase of finite clusters of bonds from a phase with an infinite cluster [1, 2].

If sites are occupied with probability p *and* bonds are occupied with probability q, we speak of site–bond percolation. Two occupied sites belong to the same cluster if they are connected by a path of nearest-neighbour occupied sites with occupied bonds in between. For $q = 1$, site–bond percolation reduces to site percolation, for $p = 1$ it reduces to bond percolation. In general, both parameters characterize the state of the system. Accordingly, a critical line in p-q space separates both phases, which for $p = 1$ and $q = 1$ takes the values of the critical bond and site concentrations, respectively.

Perhaps the most common example of bond percolation in physics is a random resistor network, where the metallic wires in a regular network are cut randomly with probability $1 - q$. Here q_c separates a conductive phase at large q from an insulating phase at low q. A possible application of bond percolation in chemistry is the polymerization process, where small branching molecules can form large molecules by activating more and more bonds between them. If the activation probability q is above the critical concentration, a network of chemical bonds spanning the whole system can be formed, while below q_c only macromolecules of finite size can be generated. This process is called a sol-gel transition. An example of this gelation process is the boiling of an egg, which at room temperature is liquid and upon heating becomes a more solid-like gel. Site–bond percolation can be relevant for gelation in dilute media.

The most natural example of percolation is continuum percolation, where the positions of the two components of a random mixture are not restricted to the discrete sites of a regular lattice. As a simple example, consider a sheet of conductive material, with circular holes punched randomly in it (see Fig. 22.5 (b)). The relevant quantity now is the fraction p of remaining conductive material. Compared with site and bond percolation, the critical concentration is further decreased: $p_c \cong 0.312$ for $d = 2$, when all circles have the same radius. This picture can easily be generalized to three dimensions, where spherical voids are generated randomly in a cube, and $p_c \cong 0.034$. Due to its similarity to Swiss cheese, this model of continuous percolation is called the Swiss cheese model. Similar models, where also the size of the spheres can vary, are used to describe sandstone and other porous materials. Often also the inverse model is considered, where the circular discs or spheres represent the conductive material [8].

It is important that close to the percolation threshold all these different percolation systems are characterized by the same critical exponents β, ν, and d_f given in Table 22.1. The exponents are universal and depend neither on the structural details of the lattice (e.g., square or triangular) nor on the type of percolation (site, bond, or continuum), but only on the dimension d of the system.
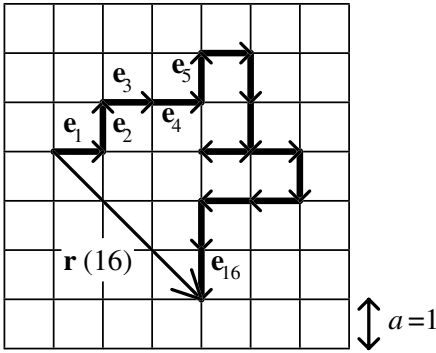
Fig. 22.6. Random walk on a square lattice. The lattice constant $a = 1$ is equal to the jump length of the random walker. Sixteen steps of the walk are shown.

22.5 Diffusion on Regular Lattices

After we have discussed the structural properties of percolation systems close to the percolation threshold, we will now focus on the *dynamical* properties of percolation systems, where to each site or bond a physical property such as conductivity is assigned. We show that due to the fractal nature of the percolation clusters near p_c, the physical laws of dynamics are changed essentially and become *anomalous*.

At first, we consider regular lattices. The diffusion process is commonly modelled by a simple random walk (see e. g., Chaps. 18 and 19), which advances one step of length a in one time unit. Each step brings the random walker to a randomly chosen nearest-neighbour site on a given d-dimensional lattice. Assume that the walker starts at time $t = 0$ at the origin of the lattice. After t time steps, the actual position is described by the vector (see Fig. 22.6)

$$\mathbf{r}(t) = a \sum_{\tau=1}^{t} \mathbf{e}_\tau, \tag{22.7}$$

where $\mathbf{e}_\tau$ denotes the unit vector pointing in the direction of the jump at the τ th time step.

The mean distance the random walker has travelled after t time steps is described by the root mean square displacement $R(t) \equiv \langle r^2(t) \rangle^{1/2}$, where the average $\langle \cdots \rangle$ is over all random-walk configurations on the lattice. From (22.7) we obtain

$$\langle r^2(t) \rangle = a^2 \sum_{\tau,\tau'=1}^{t} \langle \mathbf{e}_\tau \cdot \mathbf{e}_{\tau'} \rangle = a^2 t + \sum_{\tau \neq \tau'} \langle \mathbf{e}_\tau \cdot \mathbf{e}_{\tau'} \rangle. \tag{22.8}$$

Since jumps at different steps τ and τ' are uncorrelated, we have $\langle \mathbf{e}_\tau \cdot \mathbf{e}_{\tau'} \rangle = \delta_{\tau\tau'}$, and we obtain the Einstein relation

$$\langle r^2(t) \rangle = a^2 t, \tag{22.9}$$

which is equivalent to Fick's first law (see Chap. 10). Note that (22.9) is independent of the dimension d of the lattice.

In the general case, when the lengths of the steps of the random walker may vary, (22.9) is modified into

$$\langle r^2(t) \rangle = 2dDt, \tag{22.10}$$

where D is the diffusion coefficient. The diffusion coefficient is (approximately) related to the dc conductivity σ_{dc} by the Nernst-Einstein equation,

$$\sigma_{\mathrm{dc}} = n(e^2/k_{\mathrm{B}}T)D, \tag{22.11}$$

where n is the density and e the charge of the diffusing particles.

A more complete description of the diffusion process is possible with the probability density $P(r, t)$, which is the probability of finding the walker after t time steps at a site within distance r from its starting point. The mean square displacement can be obtained from $P(r, t)$ via $\langle r^2(t) \rangle = \int \mathrm{d}\boldsymbol{r}\, r^2 P(r, t)$. For $t \gg r$, $P(r, t)$ is described by a Gaussian: $P(r, t) \cong \frac{1}{\sqrt{2\pi t}} e^{-r^2/2t}$. This "normal" probability density – commonly referred to as the propagator (see Chaps. 10, 18, and 23) – characterizes the diffusion on regular lattices. Next we consider disordered structures.

22.6 Diffusion on Percolation Clusters

We start with the infinite percolation cluster at the critical concentration p_{c}. The cluster has loops and dangling ends, and both substructures slow down the motion of a random walker. Due to self-similarity, loops and dangling ends occur on all length scales, and therefore the motion of the random walker is slowed down on *all* length scales. The time t the walker needs to travel a distance R is no longer, as in regular systems, proportional to R^2, but scales as $t \sim R^{d_{\mathrm{w}}}$, where $d_{\mathrm{w}} > 2$ is the fractal dimension of the random walk [1,2,9]. For the mean square displacement this yields immediately

$$\langle r^2(t) \rangle \sim t^{2/d_{\mathrm{w}}}. \tag{22.12}$$

The fractal dimension d_{w} is approximately equal to $3d_{\mathrm{f}}/2$ [10]; the results of numerical simulations can be found in Table 22.1. For continuum percolation (Swiss cheese model) in $d = 3$, d_{w} is enhanced: $d_{\mathrm{w}} \cong 4.2$ [11]. Diffusion processes described by (22.12) are generally referred to as anomalous diffusion (cf. Chap. 10).

The probability density $\langle P(r, t) \rangle_N$, averaged over N percolation clusters, is not so easy to calculate. Analytical expressions for $\langle P(r, t) \rangle_N$ that fully describe the data obtained from numerical simulations can be derived. The derivation is beyond the scope of this book and we refer the interested reader to [1, 12].
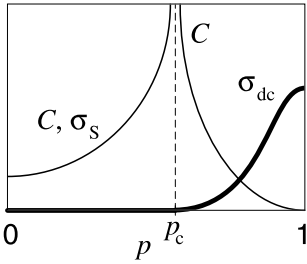
Fig. 22.7. Schematic diagram of the (usual) dc conductivity σ_{dc} (cf. (22.15), bold line) and the conductivity σ_{S} for a conductor-superconductor percolation network (cf. (22.20), thin line for $p < p_{\text{c}}$) versus the concentration p of occupied sites. The cluster capacitance C is proportional to σ_{S} for $p < p_{\text{c}}$ and diverges with the same exponent for $p > p_{\text{c}}$ (see (22.25)).

Comparatively simple, however, is the scaling behaviour of $\langle P(0, t) \rangle$, that denotes the probability of being, after t time steps, at the site where the random walker started. Since for very large times each site has the same probability of being visited, the probability of being at the origin is proportional to the inverse of the number of distinct sites $S(t)$ the random walker visited. Since $S(t)$ increases with $R(t) \equiv \langle r^2(t) \rangle^{1/2}$ as $S(t) \sim R(t)^{d_{\text{f}}}$, we have

$$\langle P(0, t) \rangle \sim R(t)^{-d_{\text{f}}} \sim t^{-d_{\text{f}}/d_{\text{w}}} \tag{22.13}$$

(see also Chap. 19). Above p_{c}, fractal structures occur only within the correlation length $\xi(p)$ from (22.2). Thus the anomalous diffusion law, (22.12), occurs only below the corresponding crossover time $t_\xi \sim R(t_\xi)^{d_{\text{w}}} \sim \xi^{d_{\text{w}}}$, which decreases proportional to $(p - p_{\text{c}})^{-\nu d_{\text{w}}}$, if p is further increased. Above t_ξ, on large time scales, the random walker explores large length scales where the cluster is homogeneous, and $\langle r^2(t) \rangle$ follows Fick's law (cf. (22.9) or (22.10)) increasing linearly with time t. Thus,

$$\langle r^2(t) \rangle \sim \begin{cases} t^{2/d_{\text{w}}}, & \text{if } t \ll t_\xi, \\ t, & \text{if } t \gg t_\xi. \end{cases} \tag{22.14}$$

22.7 Conductivity of Percolation Clusters

The diffusion coefficient is related to the dc conductivity σ_{dc} by the Nernst-Einstein equation, (22.11). Below p_{c}, there is no current between opposite edges of the system, and $\sigma_{\text{dc}} = 0$. Above p_{c}, σ_{dc} increases by a power law (see Fig. 22.7 for illustration),

$$\sigma_{\text{dc}} \sim (p - p_{\text{c}})^{\mu}, \tag{22.15}$$

where the critical exponent μ is (semi)-universal. For percolation on a lattice, μ depends only on d; the numerical results are contained in Table 22.1. For continuum percolation (Swiss cheese model) in $d = 3$, however, μ is enhanced: $\mu \cong 2.38$.

Combining (22.11) and (22.15), we can obtain the behaviour of the diffusion coefficient D as a function of $p - p_{\text{c}}$. Since only the particles on

the infinite cluster contribute to the dc conductivity, we have (from (22.1))
$n \sim P_\infty \sim (p - p_c)^\beta$ in (22.11). This yields

$$D \sim (p - p_c)^{\mu - \beta}. \tag{22.16}$$

Next we use scaling arguments to relate the exponent μ to d_w. Equations
(22.16) and (22.10) imply that above t_ξ the mean square displacement $\langle r^2(t) \rangle$
behaves as

$$\langle r^2(t) \rangle \sim (p - p_c)^{\mu - \beta} t, \quad t > t_\xi. \tag{22.17}$$

On the other hand we know that for times below t_ξ on distances $r < t_\xi^{1/d_w}$,

$$\langle r^2(t) \rangle \sim t^{2/d_w}, \quad t < t_\xi. \tag{22.18}$$

By definition, for $t = t_\xi$, we have $\langle r^2(t) \rangle \sim \xi^2$. Substituting this into
(22.17) and (22.18) and equating both relations we obtain immediately
$(p - p_c)^{\mu - \beta} t_\xi \sim t_\xi^{2/d_w}$. Using $t_\xi \sim \xi^{d_w} \sim (p - p_c)^{-\nu d_w}$ (from (22.2)) we
get the relation between μ and d_w,

$$d_w = 2 + (\mu - \beta)/\nu. \tag{22.19}$$

22.8 Further Electrical Properties

In the last section we have already seen that the dc conductivity in the
conductor-insulator system is zero below p_c and increases with a power law
above p_c. If we consider, instead, the corresponding superconductor-conduc-
tor system, the conductivity is infinite above p_c and diverges with a power
law when approaching p_c from below (see Fig. 22.7),

$$\sigma_S \sim (p_c - p)^{-s}. \tag{22.20}$$

The numerical results for s can be found in Tab. 22.1.

Next, for generalizing this result and for obtaining further electric prop-
erties, let us assume that each bond in the network represents (with proba-
bility p) a circuit consisting of a resistor with resistivity $1/\sigma_A^0$ and a capac-
itor with capacitance C_A, or (with probability $1 - p$) a circuit consisting of
a resistor with resistivity $1/\sigma_B^0$ and a capacitor with capacitance C_B. The
(complex) conductivity of each bond is therefore either $\sigma_A = \sigma_A^0 - i\omega C_A$
or $\sigma_B = \sigma_B^0 - i\omega C_B$. This model is called equivalent circuit model. At the
percolation threshold the total conductivity follows a power law [1, 13, 14],

$$\sigma(\omega) = \sigma_A(\sigma_A/\sigma_B)^{-u}, \tag{22.21}$$

where the exponent

$$u = \mu/(\mu + s) \tag{22.22}$$

is related to the exponents μ and s from above, $u = 0.5$ in $d = 2$ and $u \cong 0.71$ in $d = 3$ (see Tab. 22.1).

For extending this result to the critical regime below and above p_c, we multiply (22.21) by a complex scaling function $S(z)$ that depends on $z = |p - p_\mathrm{c}|(\sigma_\mathrm{A}/\sigma_\mathrm{B})^\Phi$ and can be different above and below p_c [15, 16],

$$\sigma(\omega) = \sigma_\mathrm{A}(\sigma_\mathrm{A}/\sigma_\mathrm{B})^{-u} \cdot S[|p - p_\mathrm{c}|(\sigma_\mathrm{A}/\sigma_\mathrm{B})^\Phi]. \qquad (22.23)$$

The exponent Φ as well as the asymptotic behaviour of the scaling function is determined by the asymptotic behaviour of $\sigma(\omega)$ in the limit $\omega \to 0$ and $(\sigma_\mathrm{A}/\sigma_\mathrm{B}) \to \infty$.

In the following, let us concentrate on the conductor-capacitor limit, where $\sigma_\mathrm{A} = \sigma_\mathrm{A}^0$ and $\sigma_\mathrm{B} = -\mathrm{i}\omega C_\mathrm{B}$. Then the complex scaling variable z is proportional to $|p - p_\mathrm{c}|[\sigma_\mathrm{A}^0/(-\mathrm{i}\omega C_\mathrm{B})]^\Phi \sim (\tau\omega)^{-\Phi}$, and $\tau = |p - p_\mathrm{c}|^{-1/\Phi}C_\mathrm{B}/\sigma_\mathrm{A}^0$ defines the characteristic time scale in this short-circuit model. Splitting the complex function $(-\mathrm{i})^u S(z)$ into its real part S_1 and imaginary part S_2, we obtain for the complex conductivity

$$\sigma(\omega) = \sigma_\mathrm{A}^0(C_\mathrm{B}/\sigma_\mathrm{A}^0)^u \cdot \omega^u \cdot [S_1(\tau\omega)] + \mathrm{i}S_2(\tau\omega)], \qquad (22.24)$$

where S_1 and S_2 are real functions.

According to standard electrodynamics, in the limit of $\omega \to 0$ the real part of the complex conductivity tends to σ_dc, while the imaginary part becomes $-\omega C$, with C the capacitance of the whole system:

$$\sigma(\omega) \to \begin{cases} \sigma_\mathrm{dc} - \mathrm{i}\omega C, & \text{if } p > p_\mathrm{c}, \\ -\mathrm{i}\omega C, & \text{if } p < p_\mathrm{c} \end{cases} \qquad (\omega \to 0). \qquad (22.25)$$

For satisfying these conditions, we must require that $S_1(\tau\omega) \sim (\tau\omega)^{-u}$ above p_c and $S_2(\tau\omega) \sim (\tau\omega)^{1-u}$ below and above p_c. The first condition determines, together with (22.15) and (22.22), the scaling exponent Φ, $\Phi = 1/(\mu + s)$. The second condition yields the new relation for the capacitance [1, 15, 16],

$$C \sim S_2(\tau\omega) \sim |p - p_\mathrm{c}|^{(u-1)/\Phi} = |p - p_\mathrm{c}|^{-s}, \qquad (22.26)$$

with the same exponent s below and above p_c (see Fig. 22.7). The divergency of C at p_c has a simple physical interpretation: each pair of neighboured clusters forms a capacitor. The effective surface increases when p_c is approached and tends to infinity at p_c. Accordingly, the effective capacitance C of the system also diverges. Next, we discuss a (non-trivial) application of the percolation concept, the ionic transport in heterogeneous ionic conductors. For a recent application of the percolation concept in gas sensors, see [17].
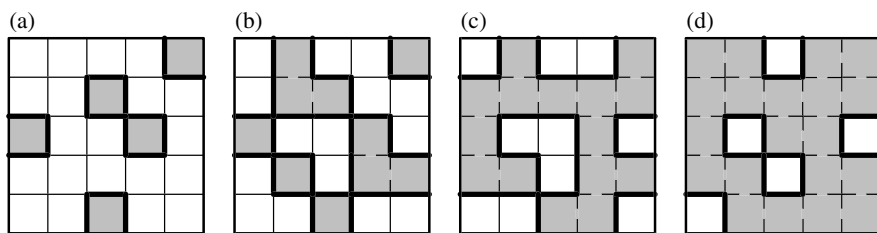
Fig. 22.8. Illustration of the three-component percolation model for dispersed ionic conductors, for different concentrations p of the insulating material. The insulator is represented by the grey area, the ionic conductor by the white area. The bonds can be highly conducting bonds (A bonds, bold lines), normal conducting bonds (B bonds, thin lines), or insulating (C bonds, dashed lines). (a) $p < p'_c$, (b) $p = p'_c$, (c) $p = p''_c$, and (d) $p > p''_c$ (redrawn after [22]).

22.9 Application of the Percolation Concept: Heterogeneous Ionic Conductors

22.9.1 Interfacial Percolation and the Liang Effect

Let us now turn to percolation models that describe electrical transport in specific composite materials. A substantial amount of research has concentrated on "dispersed ionic conductors" after the discovery by Liang [18] that insulating fine particles with sizes of the order of 1 μm, dispersed in a conductive medium (e. g. Al_2O_3 in LiI), can lead to a conductivity enhancement [19]. This effect has been found to arise from the formation of a defective, highly conducting layer following the boundaries between the conducting and the insulating phase [20]. Effectively, the system thus contains three phases. Theoretical studies therefore have focused on suitable three-component impedance network models.

Figure 22.8 shows a two-dimensional illustration of such composites in a discretized model [21, 22]. In its simplest version this model is constructed by randomly selecting a fraction p of elementary squares on a square lattice, which represent the insulating phase, while the remaining squares are the conducting phase. The distribution of both phases leads to a correlated bond percolation model with three types of bonds and associated bond conductances σ_α; $\alpha =$ A, B, C; as defined in Fig. 22.8. For example, bonds in the boundary between conducting and insulating phases correspond to the highly conducting component (A bonds). The analogous construction for three dimensions is obvious. Finite-frequency effects are readily included, when we allow bond conductances to be complex [23]. For simplicity, we may assume the ideal behaviour $\sigma_\alpha = \sigma_\alpha^0 - i\omega C_\alpha$, as in the previous section, but more general forms can be chosen when necessary. Clearly, the experimental situation described above requires that $\sigma_A^0/\sigma_B^0 = \tau \gg 1$; $\sigma_C^0 = 0$. Thereby it is
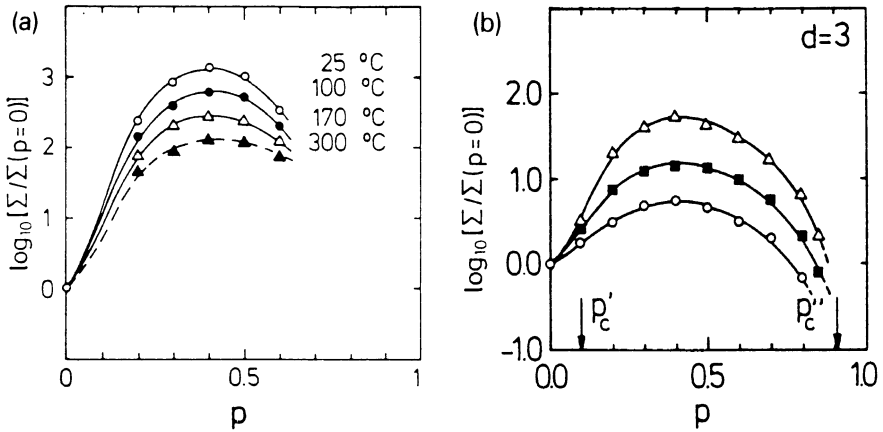
Fig. 22.9. (a) Normalized conductivity of the LiI-Al$_2$O$_3$ system as a function of the mole fraction p of Al$_2$O$_3$ at different temperatures (after [24]). (b) Normalized conductivity resulting from Monte Carlo simulations of the three-component percolation model, as a function of p, for $\sigma_A^0/\sigma_B^0 = 10$ (circles), 30 (full squares), and 100 (triangles) (after [22]).

natural to assume that σ_A^0 and σ_B^0 are thermally activated, such that their ratio $\tau \propto \exp(-\Delta E/k_B T)$ increases with decreasing temperature.

A remarkable feature of this model is the existence of two threshold concentrations. At $p = p'_c$, interface percolation (i.e., percolation of A bonds) sets in, whereas at $p = p''_c = 1 - p'_c$ (normally not accessible by experiment) the system undergoes a conductor-insulator transition. In two dimensions we have $p'_c = 0.41$, while in $d = 3$, $p'_c = 0.097$, corresponding to the threshold for second-neighbour ($d = 2$) and third-neighbour ($d = 3$) site percolation on a d-dimensional lattice, respectively. At zero frequency, the total conductivity can be obtained from Monte Carlo simulation [21, 22].

Figure 22.9 shows experimental results for LiI-Al$_2$O$_3$ at four different temperatures [24] and simulation results for $d = 3$ at three different temperatures (corresponding to $\tau = 10$, 30 and 100) [22]. Good agreement is achieved, since both plots show a broad maximum. Changing τ (by varying the temperature) offers the possibility to interpret the measured activation energies as a function of p [25] and, in principle, also to detect the critical transport behaviour associated with interface percolation. In the vicinity of p'_c it seems interesting in addition to study critical ac effects. For examples, at p'_c the effective capacitance develops a peak, whose height should scale with τ as $C_{\text{eff}} \sim \tau^{1-u}$, where $u = \mu/(\mu+s)$, see (22.21) and (22.22). Ac properties in the whole range of p-values have been calculated by renormalization group techniques [23].

Several extensions of this model are conceivable. In the case of dc transport ($\omega = 0$), the variation of the total conductivity with the size of dis-
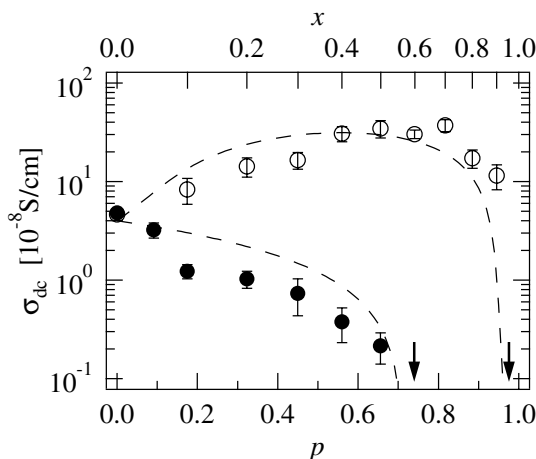
Fig. 22.10. Plot of the dc conductivity of micro- and nanocrystalline $(1 - x)\text{Li}_2\text{O}:x\text{B}_2\text{O}_3$ composites vs volume fraction p (bottom scale) and mole fraction x (top scale) of insulating B_2O_3, at $T = 433\,\text{K}$. The experimental conductivity of the nanocrystalline samples (open circles) shows an enhancement up to a maximum at $p \approx 0.7$ ($x \approx 0.5$), while the conductivity of the microcrystalline composites (full circles) decreases monotonically. The arrows indicate the compositions where the dc conductivities fall below the detection limit. The dashed lines show the dc conductivities obtained from the continuum percolation model discussed in the text (after [37, 39]).

persed particles has been calculated and successfully compared with experiments [26–29]. In particular, it was found that as the particle size decreases while the thickness of the highly conducting interfacial layer is fixed, the maximum in the total conductivity as a function of the insulator concentration p shifts to smaller values of p. The observation of conductivity maxima at very low volume fractions ($\simeq 10\%$) in certain composite electrolytes, however, was interpreted by a grain boundary mechanism within the bulk of the electrolyte phase [30].

Related work also emphasized aspects of continuum percolation in dispersed ionic conductors [27, 29], which, depending on the geometrical conditions, can lead to dynamical critical properties differing from lattice percolation (see e.g. Sect. 22.7).

22.9.2 Composite Micro- and Nanocrystalline Conductors

In the foregoing subsection, we have discussed dispersed ionic conductors that were prepared by melting the ionic conductor and adding the insulator (mainly Al_2O_3) to it. Next we consider diphase micro- and nanocrystalline materials, which were prepared by mixing the two different powders and

pressing them together to a pellet. This way, in contrast to the classic dispersed ionic conductors discussed above, the grain size of both ionic conductor and insulator can be varied over several orders of magnitude. For reviews on nanocrystalline materials, see e. g. [31–36] (cf. also Chap. 9).

Recently, the ionic conductivity of micro- and nanocrystalline $(1-x)\text{Li}_2\text{O}$: $x\text{B}_2\text{O}_3$ composites, for different contents x of insulator B_2O_3, has been studied [37–39]. In the nanocrystalline samples, with an average grain size of about 20 nm, the dc conductivity increases with increasing content of B_2O_3 up to a maximum at $x \approx 0.5$. Above 0.92, the dc conductivity vanishes.

In contrast, in the microcrystalline samples (grain size about 10 μm), the dc conductivity decreases monotonically when x is increased and seems to vanish above $x \approx 0.55$ (see Fig. 22.10). The activation energy remains almost constant in both cases, $E_\text{act} \cong 1$ eV, for all x values.

To explain these surprising experimental observations, Indris et al. [37] assumed that (as for the classical dispersed ionic conductors) (i) B_2O_3 acts as an insulator for the lithium ions, (ii) the mobility of the Li ions along the diphase boundaries between ionic conductor and B_2O_3 is larger than in the bulk lithium oxide, and (iii) that the thickness λ of this highly conducting interface is independent of the grain size.

For a quantitative treatment one has to note that the insulator content x is related to the volume fraction p (considered in percolation theory) by $p = \alpha x/(\alpha x - x + 1)$, where $\alpha = V_\text{mol}(\text{B}_2\text{O}_3)/V_\text{mol}(\text{Li}_2\text{O}) \approx 1.9065$ is the ratio between the mole volumes. Accordingly, the experimental results suggest the existence of two different percolation thresholds for the conduction paths, $p_\text{c} \approx 0.7$ for the microcrystalline samples and $p_\text{c} \approx 0.96$ for nanocrystalline ones, above which the dc conductivity of the composite vanishes.

These different thresholds can be understood by simple geometrical arguments. In the case of micro-crystalline samples, the highly conducting region at the interface between B_2O_3 and Li_2O grains does not play a role since its width is negligible compared to the grain sizes, and conducting paths can open up only when two Li_2O grains get in direct contact to each other. Qualitatively, we can expect a percolating conducting path when the Li_2O concentration gets larger than 0.3 (i.e., $p = 0.7$), which is between the percolation threshold of spheres in a three-dimensional continuum percolation model and the percolation threshold of sites in the simple cubic lattice.

In the case of nanocrystalline samples, however, the width of the highly conducting interface becomes comparable to the grain sizes. In this case, the highly conducting region can act as a bridge between two Li_2O grains not in direct contact to each other, opening up additional paths for Li ions. A percolating conducting path can be disrupted only at much higher concentrations of B_2O_3 than for micrometer sized grains. Again, the value suggested by the experiment is in the expected regime.

To describe the actual dependence of the dc conductivity of $\text{Li}_2\text{O}{:}\text{B}_2\text{O}_3$ composites, $\sigma_\text{dc}(p)$, on the insulator concentration p, Indris et al. [37] em-

ployed a continuum percolation model similar to that studied earlier for dispersed ionic conductors [27]. In this model, the size of dispersed particles is considered explicitly and the conductivity is estimated by means of the effective-medium approximation (EMA), yielding an analytical expression for $\sigma_{\mathrm{dc}}(p)$. Denoting by $P_0(p)$, $P_{\mathrm{A}}(p)$, and $P_{\mathrm{B}}(p)$ the concentrations of the insulator, the highly conducting diphase boundaries and the ionic conductor, respectively, $\sigma_{\mathrm{dc}}(p)$ is given within EMA by

$$\sigma_{\mathrm{dc}}(p) = \sigma_{\mathrm{B}}^0 \frac{1}{z-2} \left\{ -A + [A^2 + 2\tau(z - 2 - zP_0)]^{1/2} \right\}, \qquad (22.27)$$

where $A = \tau(1 - zP_{\mathrm{A}}/2) + (1 - zP_{\mathrm{B}}/2)$, z is a parameter determining the percolation threshold p_{c} at which $\sigma_{\mathrm{dc}} = 0$, and $\tau = \sigma_{\mathrm{A}}^0/\sigma_{\mathrm{B}}^0$ is (as before) the enhancement factor, defined as the ratio between the conductivities of the highly conducting interface and of pure $\mathrm{Li_2O}$, respectively. For details of the treatment, we refer to [27, 37]. The concentrations of the three components are given by $P_0(p) = p$, $P_{\mathrm{B}}(p) = (1 - p)^{\eta^3}$ and $P_{\mathrm{A}}(p) = 1 - p - P_{\mathrm{B}}(p)$, with

$$\eta = \frac{R + \lambda}{R}, \qquad (22.28)$$

where R is the radius of the particles ($R \cong 10$ nm for the nanoparticles and $R \cong 5$ μm for the microparticles) and λ between 1 and 2 nm.

According to (22.27), the percolation threshold for the disruption of conducting paths, p_{c}, is given by $p_{\mathrm{c}} = (z - 2)/z$. Thus, from our previous discussion, we expect that for nanocrystalline samples, $p_{\mathrm{c}} \approx 0.96$, obtaining $z_{\mathrm{nano}} = 59$, while in the microcrystalline case $p_{\mathrm{c}} \approx 0.7$ and $z_{\mathrm{poly}} = 7$. The remaining parameters, except the interface conductivity σ_{A}^0 can be easily estimated from the measurements. The theoretical results, obtained for a reasonable fit of σ_{A}^0, are displayed in Fig. 22.10 as dashed lines. The agreement is quantitatively good in view of the simplicity of the model employed.

Both nanocrystalline and microcrystalline materials have been described within the same model. The striking difference between both is the parameter η; $\eta - 1$ describes the thickness of the interface in relation to the grain size. For η close to one, the blocking effect of the large insulating grains dominates, and the dc conductivity decreases monotonically, while for smaller grain sizes a similar behaviour as in the classic dispersed ionic conductors occurs.

The results summarized here are consistent with results of nuclear magnetic resonance studies on the same composites, presented in Sect. 9.6.4 of Chap. 9.

22.10 Conclusion

In this chapter we gave a short introduction to the standard model for disordered systems, the percolation model. Percolation clusters at the critical

concentration are self-similar on all length scales and their structure as well as several substructures can be described with the concept of fractal dimensions. Because the clusters have loops and dangling ends on all length scales diffusion processes on these structures are slowed down and become anomalous. Diffusion is related to electrical conductivity via the Nernst-Einstein relation, and thus the scaling behaviour of the dc conductivity can be deduced from it. Other scaling arguments give the dependence of the capacity on the concentration of conducting sites, and show that the capacity diverges at the percolation threshold. In the last section, we reviewed experimental results and numerical simulations for ionic conduction in heterogeneous ionic conductors.

Notation

C	capacitance
D	diffusion coefficient
M	cluster mass
p, q	concentration of occupied sites, resp. bonds
p_c, q_c	critical concentrations (percolation thresholds)
P_∞	concentration of sites from infinite cluster
$P(r, t)$	probability density of random walk
r, ℓ	Euclidean and topological (chemical) distance
$R(t) \equiv \langle r^2(t) \rangle^{1/2}$	root mean square displacement of random walk
ξ	correlation length
σ_{dc}	dc conductivity
σ_S	conductivity in conductor-superconductor system

References

1. *Fractals and Disordered Systems*, 2nd edn, ed by A. Bunde, S. Havlin (Springer, Berlin Heidelberg New York 1996)
2. D. Stauffer, A. Aharony: *Introduction to Percolation Theory* (Taylor & Francis, London 1992)
3. G.R. von Grimmett: *Percolation*, 2nd edn (Springer, Berlin Heidelberg New York 1999)
4. M. Sahimi: *Application of Percolation Theory* (Taylor & Francis, London 1994)
5. A. von Hunt: *Percolation Theory for Flow in Porous Media*, Lecture Notes in Physics, vol 674 (Springer, Berlin Heidelberg New York 2005)
6. P. Grassberger: J. Phys. A **25**, 5475 (1992)
7. P. Grassberger: Physica A **262**, 251 (1999)
8. C.D. Lorenz, R.M. Ziff: J. Chem. Phys. **114**, 3659 (2001)
9. D. BenAvraham, S. Havlin: *Diffusion and Reactions in Fractals and Disordered Systems* (Cambridge University Press, Cambridge 2005)
10. S. Alexander, R.L. Orbach: J. Phys. Lett. (Paris) **43**, L625 (1982)
11. S. Feng, B.I. Halperin, P. Sen: Phys. Rev. B **35**, 197 (1987)

12. A. Bunde, J. Dräger: Phys. Rev. E **52**, 53 (1995)
13. A.M. Dykne: Zh. Eksp. Theor. Fiz. **59**, 110 (1970); Sov. Phys. JETP **32**, 63 (1971)
14. J.P. Straley: J. Phys. C **9**, 783 (1976); Phys. Rev. B **15**, 5733 (1977)
15. A.L. Efros, B.I. Shklovskii: Phys. Stat. Sol. B **76**, 475 (1976)
16. D. Stroud, D.J. Bergman: Phys. Rev. B **25**, 2061 (1982)
17. M. Ulrich, A. Bunde, C.-D. Kohl: Appl. Phys. Lett. **85**, 242 (2004)
18. C.C. Liang: J. Electrochem. Soc. **120**, 1289 (1973)
19. For a review see: A.K. Shukla, V. Sharma. In: *Solid State Ionics: Materials Applications*, ed by B.V.R. Chowdari, S. Chandra, S. Singh, P.C. Srivastava (World Scientific, Singapore 1992) p 91
20. J. Maier. In: *Superionic Solids and Electrolytes*, ed by A.L. Laskar, S. Chandra (Academic Press, New York 1989) p 137
21. A. Bunde, W. Dieterich, H.E. Roman: Phys. Rev. Lett. **55**, 5 (1985)
22. H.E. Roman, A. Bunde, W. Dieterich: Phys. Rev. B **34**, 3439 (1986)
23. R. Blender, W. Dieterich: J. Phys. C **20**, 6113 (1987)
24. F.W. Poulsen, N.H. Andersen, B. Kindl, J. Schoonman: Solid State Ionics **9/10**, 119 (1983)
25. C. Li-Quan, Z. Zong-Yuan, W. Chao-Ying, L. Zi-Rong: Acta Phys. Sin. **34**, 1027 (1984)
26. H.E. Roman, M. Yussouff: Phys. Rev. B **36**, 7285 (1987)
27. H.E. Roman: J. Phys.: Condens. Matter **2**, 3909 (1990)
28. G.M. Zhang: Phys. Rev. B **53**, 6256 (1996)
29. B. Roling, S. Murugavel: Z. Phys. Chem. **219**, 23 (2005)
30. A.J. Bhattacharya, T. Dutta, S. Roy, S. Tarafdar, T.R. Middya. In: *Materials Science Forum 223–224*, ed by D.K. Chaturvedi, G.E. Murch (Trans Tech Publications, Switzerland 1996) p 279
31. H. Gleiter: Progress in Materials Science **33**, 223 (1989)
32. J. Maier: Prog. Solid State Chem. **23**, 171 (1995)
33. *Amorphous and Nanocrystalline Materials*, Advances in Materials Research, vol 3, ed by A. Inoue, K. Hashimoto (Springer, Berlin Heidelberg New York 2001)
34. J. Jamnik, J. Maier: Phys. Chem. Chem. Phys. **5**, 5215 (2003)
35. P. Heitjans, S. Indris: J. Phys.: Condens. Matter **15**, R1257 (2003)
36. V.V. Kharton, F.M.B. Marques, A. Atkinson: Solid State Ionics **174**, 135 (2004)
37. S. Indris, P. Heitjans, H.E. Roman, A. Bunde: Phys. Rev. Lett. **84**, 2889 (2000)
38. M. Ulrich, A. Bunde, S. Indris, P. Heitjans: Phys. Chem. Chem. Phys. **6**, 3680 (2004)
39. S. Indris, P. Heitjans, M. Ulrich, A. Bunde: Z. Phys. Chem. **219**, 89 (2005)